Geophysical Prospecting

EAGE EUROPEAN ASSOCIATION OF GEOSCIENTISTS & ENGINEERS

Geophysical Prospecting, 2016, **64**, 1524–1536 doi: 10.1111/1365-2478.12265

Physical constraints on c_{13} and δ for transversely isotropic hydrocarbon source rocks

Fuyong Yan, De-Hua Han and Qiuliang Yao

Rock Physics Laboratory, University of Houston, Houston, TX 77204-5007

Received December 2013, revision accepted January 2015

ABSTRACT

Based on the theory of anisotropic elasticity and observation of static mechanic measurement of transversely isotropic hydrocarbon source rocks or rock-like materials, we reasoned that one of the three principal Poisson's ratios of transversely isotropic hydrocarbon source rocks should always be greater than the other two and they should be generally positive. From these relations, we derived tight physical constraints on c_{13}, Thomsen parameter δ, and anellipticity parameter η. Some of the published data from laboratory velocity anisotropy measurement are lying outside of the constraints. We analysed that they are primarily caused by substantial uncertainty associated with the oblique velocity measurement. These physical constraints will be useful for our understanding of Thomsen parameter δ, data quality checking, and predicting δ from measurements perpendicular and parallel to the symmetrical axis of transversely isotropic medium. The physical constraints should also have potential application in anisotropic seismic data processing.

Key words: Anisotropy, velocity measurement, Poisson's ratios, Elastic constants, Thomsen parameters δ.

INTRODUCTION

Thomsen (1986) defined a set of parameters (ε, γ, and δ) and brought up weak anisotropy approximations for the phase velocities in a transversely isotropic (TI) medium. These parameters and the linearized approximation are widely accepted and used in the industry. With increasing importance of organic shale as a reservoir rock, laboratory velocity anisotropy measurements on shales are done routinely. The results are usually reported in terms of Thomsen parameters (Vernik and Nur 1992; Johnston and Christensen 1995; Vernik and Liu 1997; Jakobsen and Johansen 2000; Sondergeld *et al.* 2000; Wang 2002a, 2002b; Sondergeld and Rai 2011; Sone 2012). Of the three parameters, δ is one of the most important parameters for exploration geophysicists since it describes the relation between the normal moveout velocity and the vertical velocity (Thomsen 1986; Tsvankin 2012). Thomsen (1986) pointed out that δ is an "awkward" combination of elastic parameters and its physical meaning is not straightforward. In spite of a large amount of laboratory measurement, our understanding of parameter δ is still not quite clear (Banik 1987; Sayers 2004). The laboratory measurement found that δ has very poor correlation with other Thomsen parameters, and even the rational data range of δ is not certain.

Of the five independent elastic constants (c_{11}, c_{33}, c_{44}, c_{66}, and c_{13}) of a TI medium, although theoretically they are free independent variables, good to excellent mutual correlations are found existing between c_{11} and c_{66} and between c_{33} and c_{44} from laboratory velocity anisotropy measurements on hydrocarbon source rocks samples. Nevertheless, the behaviour of c_{13} is erratic. The correlations between c_{13} and the other elastic constants are usually very poor. This might be because estimation of c_{13} from oblique velocity measurement introduces extra uncertainties compared with traditional ultrasonic measurement. We believe that, for TI hydrocarbon source rocks, there should exist some forms of constraints on c_{13} if the elastic properties in directions perpendicular and parallel to the symmetry axis are known. If we know the behaviour of c_{13}, then we can constrain Thomsen parameter δ.

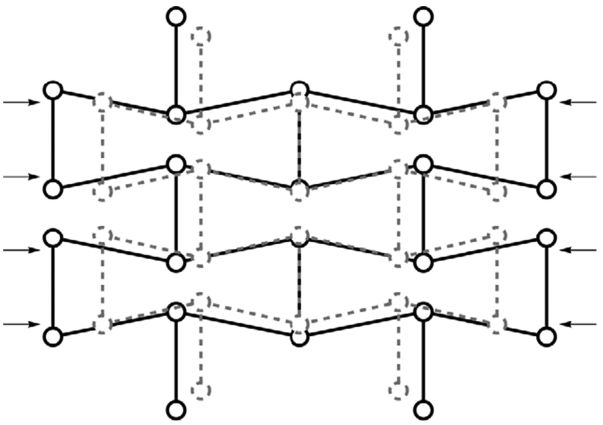

Figure 1 Network structure of a material with negative Poisson's ratio (after Lakes (1991) and Dmitriev, Shigenari, and Abe (2001)). Grey dashed lines and circles represent the deformed network under axial compression.

THEORY

Young's modulus (E) and Poisson's ratio (ν) are basic parameters to describe the mechanical properties of materials. For the isotropic medium, from the definitions and using Hooke's law, they are related to the elastic constants as follows (Mavko, Mukerji, and Dvorkin 1998):

$$E = \frac{9K\mu}{3K+\mu}, \quad \nu = \frac{3K-2\mu}{2(3K+\mu)} = \frac{3\lambda}{2(3K+\mu)}. \tag{1}$$

where K is the bulk modulus, μ is the shear modulus, and λ is the Lamé parameter. The theoretical value of ν lies between [-1, 0.5] (Landau and Lifshitz 1970; Thomsen 1990; Carcione and Cavallini 2002). The Poisson's ratio of common natural material is positive. Materials of negative materials were believed to be non-existing (Landau and Lifshitz 1970), but they do exist. Materials of negative Poisson's ratio are called "auxetic" materials and have important applications nowadays (Evans *et al.* 1991; Greaves *et al.* 2011). Most of the auxetic materials are synthetic and have special network structures. Figure 1 shows one of the deformation mechanisms leading to negative Poisson's ratio. This kind of network structure is rarely found in natural rocks. For natural isotropic rock, practical limits of Poisson's ratios are given as 0 at the low side and is theoretically by 0.5 at the high side(Gercek 2007).

The concepts of Young's modulus and Poisson's ratio can be straightforwardly extended to TI medium using Hooke's law (King 1964; Banik 2012). Their relations with the elastic constants are as follows:

$$E_V = \frac{c_{33}(c_{11}-c_{66})-c_{13}^2}{c_{11}-c_{66}}, \quad (= E_3), \tag{2}$$

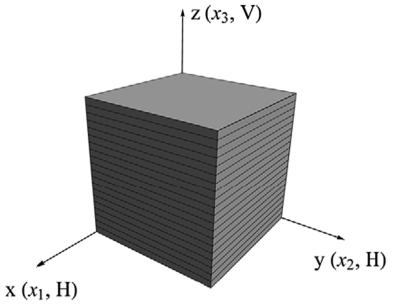

Figure 2 The right-hand coordinate system used for notation in this study.

$$E_H = \frac{4c_{66}(c_{33}(c_{11}-c_{66})-c_{13}^2)}{c_{11}c_{33}-c_{13}^2}, \quad (= E_1 = E_2), \tag{3}$$

$$\nu_V = \frac{c_{13}}{2(c_{11}-c_{66})}, \quad (= \nu_{31} = \nu_{32}), \tag{4}$$

$$\nu_{HV} = \frac{2c_{13}c_{66}}{c_{11}c_{33}-c_{13}^2}, \quad (= \nu_{13} = \nu_{23}), \tag{5}$$

$$\nu_{HH} = \frac{c_{33}(c_{11}-2c_{66})-c_{13}^2}{c_{11}c_{33}-c_{13}^2}, \quad (= \nu_{12} = \nu_{21}), \tag{6}$$

The coordinate system used for the notation is shown in Fig. 2.

An important relation exists between ν_V and ν_{HV}:

$$\frac{\nu_{HV}}{\nu_V} = \frac{E_H}{E_V}. \tag{7}$$

For hydrocarbon source rock with TI anisotropy, the Young's modulus in the horizontal direction (parallel to the bedding direction) should always be greater than that along the TI symmetry axis ($E_H > E_V$) so that $\nu_{HV} > \nu_V$.

PHYSICAL CONSTRAINTS ON c_{13} AND δ

Figure 3 shows the schematic views of the deformation of a vertical plug and a horizontal plug of organic shale under axial compression test. From the left panel, the transversal deformation is identical in every direction, and there is only one Poisson's ratio (ν_V). It is physically intuitional that the plug will not shrink transversely under axial compression, and ν_V is positive. From equation (4) and $c_{11} > c_{66}$ for a TI medium (Dellinger 1991), we get

$$c_{13} > 0. \tag{8}$$

In the right panel of Fig. 3, when a horizontal plug is under uniform axial compression, the deformation in transversal

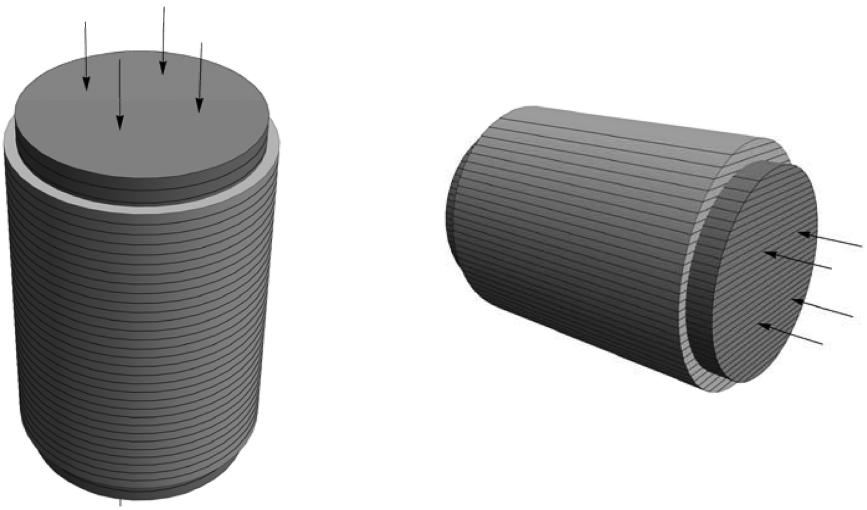

Figure 3 Schema of deformation of vertical plug (left) and horizontal plug (right) of organic shale under axial compressional testing. Dark grey represents plugs before deformation, and light grey represents plugs after deformation.

directions will not be uniform. There are two principal Poisson's ratios: ν_{HH} and ν_{HV}. Since hydrocarbon source rocks are usually stiffer in the horizontal direction (along the bedding) than in the vertical direction (perpendicular to the bedding) ($E_H > E_V$), when under axial compression, the rock is more resistant to deformation (expansion) in the horizontal direction than in the vertical direction. Thus we have $\nu_{HH} < \nu_{HV}$. If there are fractures perpendicular to the bedding, then it may lead to $\nu_{HH} > \nu_{HV}$. In this case, the effective medium does not really belong to TI medium. The TI media we considered here are referred to the clastic sediments with TI anisotropy primarily caused by layering effect and preferred orientation of minerals and cracks. If a horizontal plug of this type of media is under uniform axial compression, the passive expansion in the transverse direction is a matter of more (perpendicular to the bedding) or less (along the bedding). There is no compression force in transverse directions according to the definition of Poisson's ratio. The rock does not have the special network structure leading to negative Poisson's ratio. Therefore, there should be no shrinkage in transverse directions. From the above analysis, for hydrocarbon source rocks with TI anisotropy, we have:

$$0 < \nu_{HH} < \nu_{HV}. \tag{9}$$

This inequality is the fundamental relation to be used for the derivation of the physical constraints on c_{13}. It is validated by laboratory static mechanic measurement, as shown in Fig. 4. There is an obvious pattern of $0 < \nu_{HH} < \nu_{HV}$. Most of the samples are from organic shales. Here the Sone's data (Sone 2012) are all from static measurement on organic shales. Each pair of ν_{HH} and ν_{HV} is measured on a single horizontal

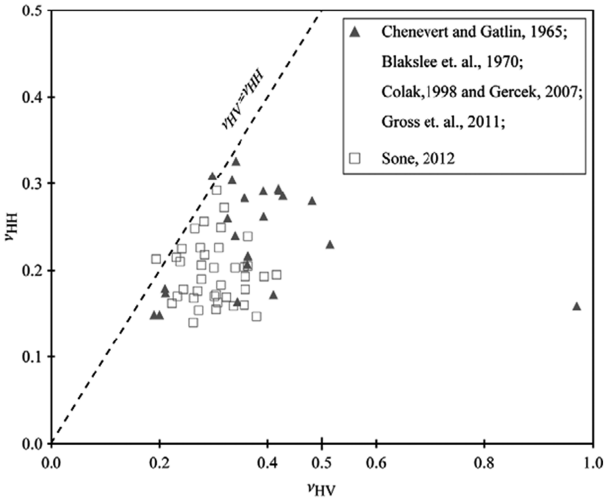

Figure 4 Static mechanic measurement of Poisson's ratios on organic shales and rock-like materials with TI anisotropy.

plug. Several samples of synthetic rock-like material with TI anisotropy are included to demonstrate that ν_{HV} can be higher than the high limit of Poisson's ratio (0.5) for the isotropic medium. If a TI medium is infinitely stronger in the horizontal direction compared with the vertical direction, then $\nu_{HV} \to 1$. The two data points showing ν_{HH} slightly higher than ν_{HV} might be caused by measurement uncertainty, and it is also possible that the material should not be classified as a TI medium. We have discussed with Hiroki Sone about the measurement uncertainty associated with the data point having higher ν_{HH} than ν_{HV} in his dataset. This data point is from Barnett-2 (Sone 2012, 2013). It has a dry bulk density of 2.65 g/cc and has weak anisotropy. It is the stiffest rock in

his data set, which means that there might be a bigger error in estimation of the strains and the Poisson's ratios. The difference betweenv_{HH} and v_{HV} for this data point is not significant and can be treated as a measurement error.

From equations (5) and (8) and $v_{HV} > 0$, we have

$$c_{11}c_{33} - c_{13}^2 > 0. \tag{10}$$

From equations (6) and (10) and $v_{HH} > 0$, if c_{13} is a real number and it exists, we must have $c_{11} - 2c_{66} > 0$, and we also have

$$c_{13} < \sqrt{c_{33}(c_{11} - 2c_{66})}. \tag{11}$$

From equations (5), (6), and (10) and $v_{HH} < v_{HV}$ we have

$$c_{13} > \sqrt{c_{33}(c_{11} - 2c_{66}) + c_{66}^2} - c_{66}. \tag{12}$$

Combining equations (11) and (12), we put the constraints on c_{13} for hydrocarbon source rocks in a neat form:

$$\sqrt{c_{33}c_{12} + c_{66}^2} - c_{66} < c_{13} < \sqrt{c_{33}c_{12}}. \tag{13}$$

When transverse isotropy reduces to isotropy ($c_{11} \to c_{33}$ and $c_{66} \to c_{44}$), the low bound is equal to $c_{33} - 2c_{44}$(for the isotropic medium: $c_{13} = c_{33} - 2c_{44}$), and the upper inequality reduces to

$$K - \frac{2}{3}\mu > 0 \quad \text{or} \quad \lambda > 0, \tag{14}$$

which is consistent with the practical limits of Poisson's ratio for natural isotropic rocks as we discussed earlier in this study.

Thomsen parameter δ is defined as (Thomsen 1986):

$$\delta = \frac{(c_{13} + c_{44})^2 - (c_{33} - c_{44})^2}{2c_{33}(c_{33} - c_{44})}. \tag{15}$$

If δ is treated as a function of c_{13}, the general shape of the curve is a parabolic curve concaving upward, as shown in Fig. 5. Here we assume that $c_{33} > c_{44}$, which means that the P-wave velocity is greater than the S-wave velocity in the symmetry direction. It can be seen that δ monotonically increases with c_{13} when $c_{13} > -c_{44}$; thus, substituting the inequality (13) into equation (15) and using Thomsen's (1986) notation, we can get the constraints for δ

$$\delta^- < \delta < \delta^+, \tag{16}$$

where

$$\delta^- = \frac{\varepsilon - 2r_0^2\gamma(1 - r_0^2(1 + 2\gamma) + \sqrt{(1 - r_0^2(1 + 2\gamma))^2 + 2\varepsilon})}{1 - r_0^2},$$

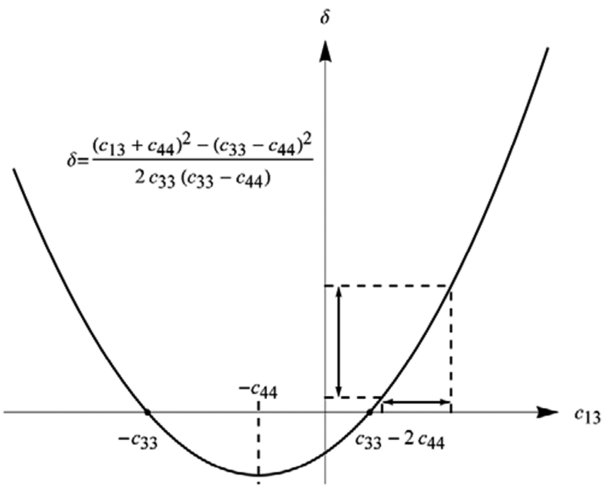

Figure 5 Relation between constraints on c_{13} and constraints on Thomsen parameter δ. (Parameters used for illustration: c_{11}=70 GPa, c_{33}=40 GPa, c_{44}=15 GPa, and c_{66}=25 GPa).

$$\delta^+ = \frac{\varepsilon - 2r_0^2\gamma + r_0^2\sqrt{1 - 2r_0^2(1 + 2\gamma) + 2\varepsilon}}{1 - r_0^2},$$

where $r_0 = \beta_0/\alpha_0$, β_0 and α_0 are the shear velocity and P-wave velocity along the TI symmetry axis, respectively. ε and γ are defined by (Thomsen 1986)

$$\varepsilon = \frac{c_{11} - c_{33}}{2c_{33}}, \quad \gamma = \frac{c_{66} - c_{44}}{2c_{44}}. \tag{17}$$

One sees that δ is constrained by other Thomsen parameters, which are all properties in directions perpendicular and parallel to the TI symmetry axis.

Alkhalifah and Tsvankin (1995) defined "anellipticity" parameter (η) that describes the degree of deviation from elliptic anisotropy:

$$\eta = \frac{\varepsilon - \delta}{1 + 2\delta}. \tag{18}$$

The anellipticity parameter η is important for anisotropic seismic data processing because it determines the relation between the normal moveout velocity and the horizontal velocity (Tsvankin 2012). In terms of elastic constants, it is equal to

$$\eta = \frac{1}{2}\left(\frac{c_{11}(c_{33} - c_{44})}{(c_{13} + c_{44})^2 + c_{44}(c_{33} - c_{44})} - 1\right). \tag{19}$$

Similarly, as shown in Fig. 6, if we know the constraints on c_{13}, the constraints on anellipticity parameter η can be determined by substituting the inequality (13) into equation (19):

$$\eta^- < \eta < \eta^+, \tag{20}$$

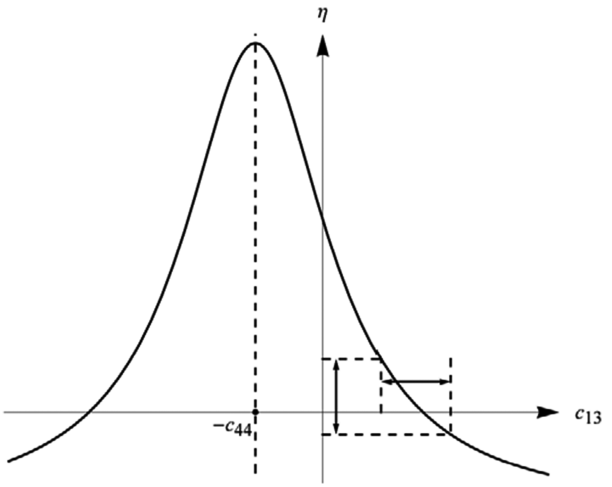

Figure 6 Relation between constraints on c_{13} and constraints on anellipticity parameter η. (Parameters used for illustration: c_{11}=70 GPa, c_{33}=40 GPa, c_{44}=15 GPa, and c_{66}=25 GPa).

where

$$\eta^{-} = \frac{r_0^2((\varepsilon - 2\gamma) + \sqrt{1 - 2r_0^2(1+2\gamma) + 2\varepsilon})}{r_0^2(1+4\gamma) - (1+2\varepsilon) - 2r_0^2\sqrt{1 - 2r_0^2(1+2\gamma) + 2\varepsilon}},$$

$$\eta^{+} = \frac{r_0^2((\varepsilon - 2\gamma) + 2\gamma(r_0^2(1+2\gamma) - \sqrt{(1 - r_0^2(1+2\gamma))^2 + 2\varepsilon}))}{r_0^2(1+4\gamma) - (1+2\varepsilon) - 4r_0^2\gamma(r_0^2(1+2\gamma - \sqrt{(1 - r_0^2(1+2\gamma))^2 + 2\varepsilon})}.$$

It can also be derived by substituting the constraints on δ(equation (16)) directly into equation (18). Obviously, the high bound of δ corresponds to the low bound of η.

LABORATORY DATA AND THE CONSTRAINTS

Figure 7 shows the crossplot between δ and v_{HH}/v_{HV} ratio from ultrasonic velocity anisotropy measurement. The data sources are from Thomsen (1986), Johnston and Christensen (1995), Vernik and Liu (1997), Jakobsen and Johansen (2000), Wang (2002b, shale and coal samples only), and Sone (2012, 2013). The data collected by Thomsen (1986) are from various sources; only data points with anisotropy obviously stronger than the measurement uncertainty ($\varepsilon > 0.03$ and $\gamma > 0.03$) are included. Wang's data are corrected for mistaking group velocity for phase velocity in the oblique direction. If there is pressure-dependent measurement, no more than three data points are selected to prevent overweighting effect of this sample. The crossplot is divided into three areas. In the left, several data points have negative v_{HH} values. The corresponding c_{13} values are above the high bound, and they

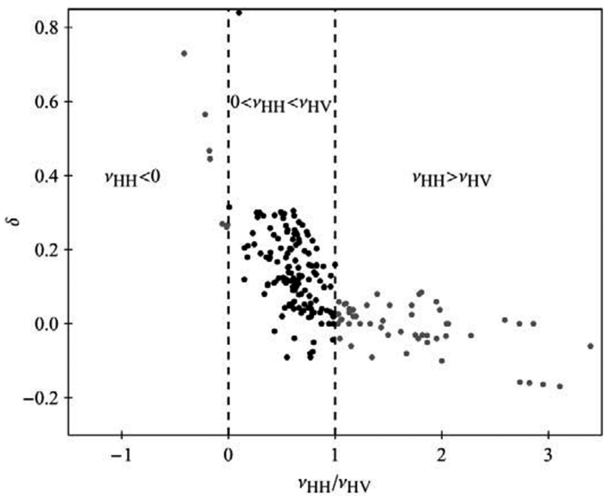

Figure 7 Crossplot between δ and v_{HH}/v_{HV} ratio from dynamic velocity anisotropy measurement. Black points (137) are within the physical bounds, and grey points (66) are outside of the bounds (data sources: Thomsen (1986), Johnston and Christensen (1995), Vernik and Liu (1997), Jakobsen and Johansen (2000), Wang (2002b), and Sone (2012)).

tend to have higher values of δ . In the right area, there are quite a few points with $v_{HH} > v_{HV}$. The corresponding c_{13} values are lower than the low bound, and they tend to have lower values of δ. About two-thirds of the data points lie in the centre area, where we believe that all the hydrocarbon source rocks with TI anisotropy should lie within. The gray point in the center area has negative value of $c_{11} - 2c_{66}$, which might be nonphysical as we will discuss later. Since there are much more data points lying below the low bound than above the high bound, there might be a general tendency of underestimating δ. For clarity, we emphasise that the constraints for c_{13} or δ might be different for each data point. Since these constraints are derived from the relation between the Poisson's ratios, the ratio of Poisson's ratios can be directly used to check whether a data point lies within or outside of the bounds of c_{13} or δ. Next, we will analyse that most of data points lying outside of bounds might be due to uncertainty in laboratory velocity anisotropy measurement.

UNCERTAINTY IN LABORATORY VELOCITY ANISOTROPY MEASUREMENT

Laboratory velocity anisotropy measurement on TI media requires at least five velocity component measurements, among which one velocity measurement must be made in oblique direction. Traditionally this oblique velocity measurement is

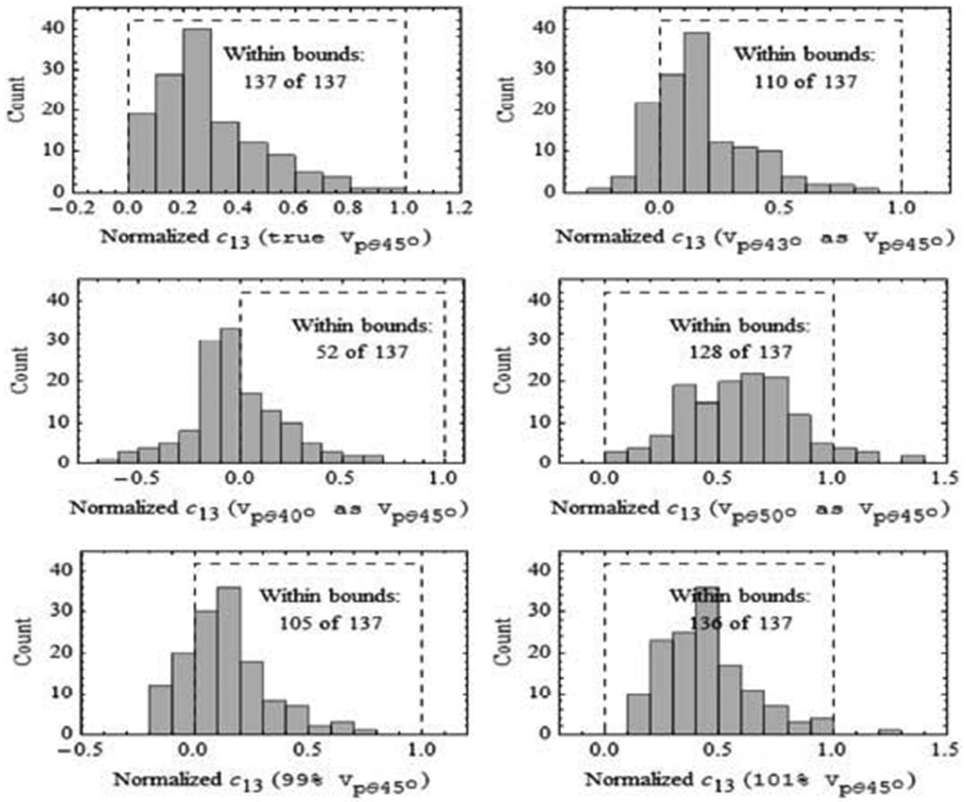

Figure 8 Sensitivity analysis: effect of angle error and velocity error on the estimation of c_{13}.

made on a 45° plug (the angle between the axial direction of the cylindrical plug and the TI symmetry axis is 45°). Taking exact 45° plug is difficult in practice, but people often ignore the angle error because the formula to calculate c_{13} is simpler if the angle is 45° or the exact angle is difficult to measure. If the real phase angle θ is not equal to 45°, then c_{13} should be calculated by

$$c_{13} = 2\csc 2\theta\sqrt{(\rho V_{P\theta}^2 - c_{11}\sin^2\theta - c_{44}\cos^2\theta)(\rho V_{P\theta}^2 - c_{33}\cos^2\theta - c_{44}\sin^2\theta)} - c_{44}. \quad (21)$$

where $V_{P\theta}$ is the phase velocity. As Yan, Han, and Yao (2012) pointed out, this small angle error can have significant effect on estimation of c_{13} and δ. In Fig. 7, we take only data points satisfying $0 < v_{HH} < v_{HV}$ and assume that the true TI elastic properties are measured. Then taking the phase velocity at phase angles 43°, 40°, and 50°, respectively, as phase velocity at phase angle 45°, we recalculate c_{13} and check how much difference is made. For display convenience, c_{13} is normalized by

$$c_{13n} = \frac{c_{13} - c_{13}^-}{c_{13}^+ - c_{13}^-}, \quad (22)$$

where

$$c_{13}^- = \sqrt{c_{33}(c_{11} - 2c_{66}) + c_{66}^2} - c_{66},$$

$$c_{13}^+ = \sqrt{c_{33}(c_{11} - 2c_{66})}.$$

If c_{13n} does not lie between 0 and 1, it is outside of the bounds. As we can see in Fig. 8, negative 2° angle error can make about 20% of the data points lie below the low bound; negative 5° angle error can make about 62% of the data points lie below the low bound; and positive 5° angle error can make about less than 8% of the data points lie above the high bound. In the bottom two panels of Fig. 8, we show the sensitivity of velocity measurement error on c_{13n}. If the phase velocity in 45° is underestimated by 1%, 22% of the data points move below the low bound. If the phase velocity in 45° is overestimated by 1%, only one data point moves above the high bound. The above sensitivity analyses partially demonstrate why there are more data points lying below the low bound than above the high bound, as shown in Fig. 7.

Another important issue is the difference between group and phase velocities. Dellinger and Vernik (1994) discussed

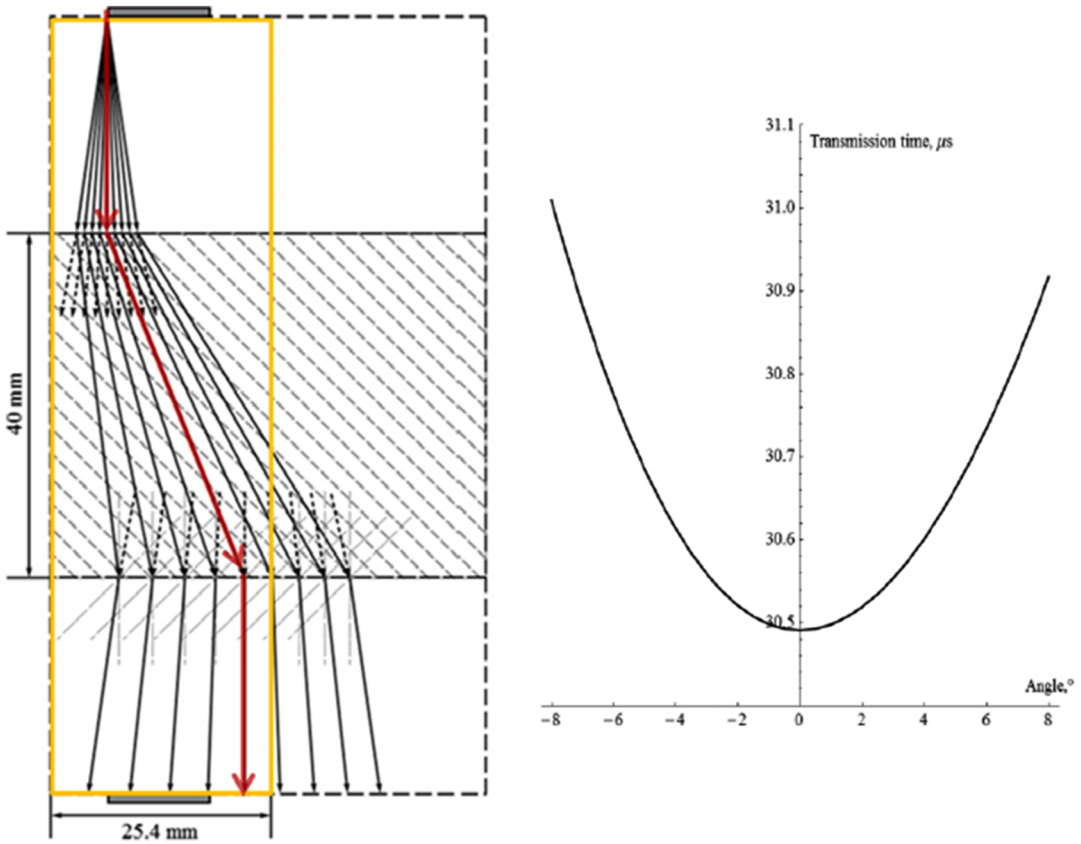

Figure 9 Use of Snell's law to simulate ultrasonic velocity measurement on a 45° plug with 1-inch diameter. The transducer dimension (diameter) is 12 mm. The left panel shows the ray tracing from the left corner of the top transducer, and the right panel shows the corresponding transmission travel times of different rays. In the TI medium, the dashed arrow denotes phase direction and the firm arrow denotes ray direction. The long dashed thin straight lines denote the TI symmetry or reflection symmetry plane. The TI elastic properties are taken as the first sample (at 8634 ft) from the dataset by Vernik and Liu (1997). The right panel shows the transmission travel time of rays in the left panel. The minimum travel time is for the vertical incident ray (in red).

related problems associated with traditional triple-plug velocity anisotropy measurement. Using Snell's law for the TI medium (Slawinski *et al.* 2000), Fig. 9 shows the ray tracing of ultrasonic velocity measurement on the 45° plug. In the TI medium, Snell's law is still consistent with Fermat's principle; this is to say that, between the emission transducer plane and the receiver transducer plane, the ray with minimum travel time (the vertical incident ray) obeys Snell's law, and it does not necessarily have the shortest path. As shown in Fig. 9, if the transducer is not wide enough (or the sample is too long), the first arriving energy might be missed by the receiving transducer and the phase velocity tends to be underestimated. In practice, the transducers need to be at least 10% wider than the minimum width so that the first-arrival signal can be strong enough for reliable breaktime picking.

After c_{11}, c_{33}, and c_{44} are known from non-oblique velocity measurement, c_{13} can be calculated by

$$c_{13} = \sqrt{\left(2\rho V_{P\theta 45^\circ}^2 - c_{11} - c_{44}\right)\left(2\rho V_{P\theta 45^\circ}^2 - c_{33} - c_{44}\right)} - c_{44}, \tag{23}$$

where $V_{P\theta 45^\circ}$ is the 45° phase velocity. In practice, $V_{P\theta 45^\circ}$ is usually greater than the P-wave velocity and the S-wave velocity along the TI symmetry axis; hence, the second term under the square root signal should always be positive, which requires that the first term must be positive as well (If not, c_{13} will be a complex number). Therefore, underestimation of the phase velocity $V_{P\theta 45^\circ}$ will cause underestimation of c_{13}, and sometimes, it even leads to negative or even complex value of

c_{13}. As shown in Fig. 5, δ is positively correlated with c_{13}, so it will be underestimated as well. Most of the velocity anisotropy data cited in this study are based on the measurement of cylindrical plugs of 1-inch diameter. The lengths of the plugs are often around 4 cm, which can be longer if the plugs are also needed for static measurement. Therefore, there might be a bias toward underestimation of c_{13} in the published velocity anisotropy measurement data.

To improve measurement efficiency, Wang (2002a) used a setup based on a single horizontal plug. An oblique velocity must be measured, which is actually group velocity. To calculate c_{13} and δ, we need to convert the group velocity to phase velocity and find the corresponding phase angle, and then use equation (21) to calculate c_{13} . Figure 10 shows group to phase correction effect on c_{13} and δ. It can be seen that, if group velocity is mistook for phase velocity, c_{13} and δ will be systematically underestimated.

The above analyses explain that why there are more data points lying below the physical constraints of c_{13} and δ than above the constraints. The data points out of the bounds might be also due to some other factors. For example, the sample has fractures crossing the bedding, which might lead to $v_{HH} > v_{HV}$. Some samples might have significant heterogeneity on the core plug scale. We sometimes find that the "horizontal" plug is not really "horizontal": the angle between the bedding and the cylindrical plug axial direction might be more than 5°. In addition, identification of the bedding direction is not always straightforward by naked eyes, and multiple oblique velocity measurements might be needed to identify the bedding direction (Yan, Han, and Yao 2014). In these cases, either the samples do not really belong to the TI medium or the measured elastic properties are apparent properties.

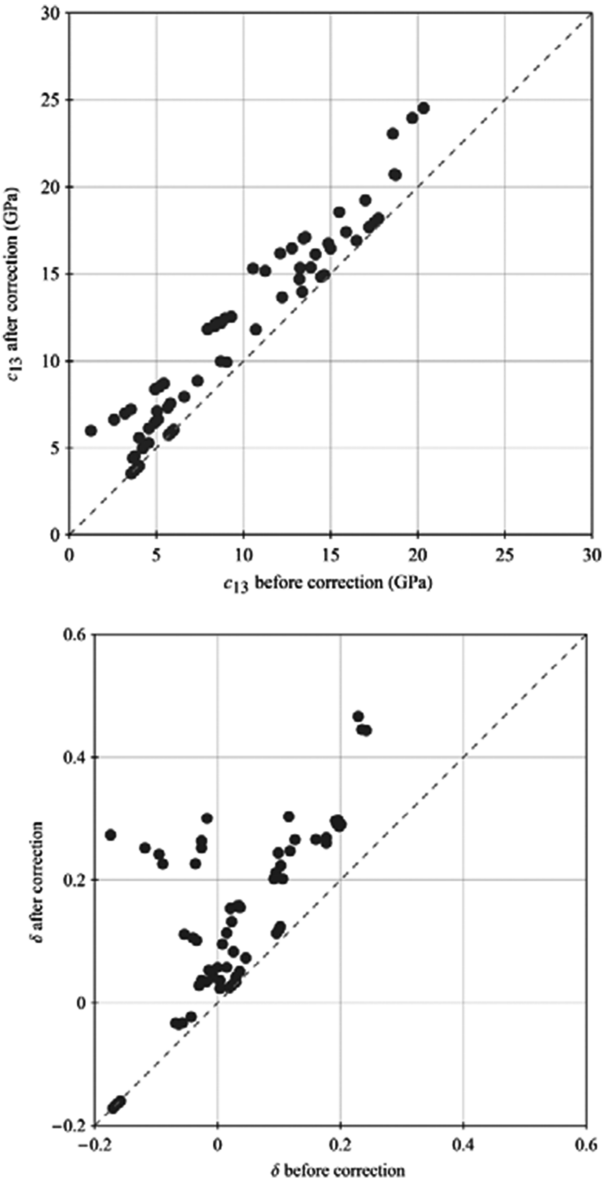

Figure 10 Phase to group correction effect on c_{13}(above) and Thomsen parameter δ(below) using Wang's data (shale and coal samples only, Wang (2002b)).

APPLICATIONS

The physical constraints can help us understand the effect of the other Thomsen parameters on δ. In Fig. 11, the δ constraints are plotted as function of β_0/α_0. The range of β_0/α_0 is selected based on laboratory anisotropy measurement on hydrocarbon source rocks. As shown in Fig. 12(a), the β_0/α_0 ratios for shales are distributed around a narrow range of 0.5–0.7. The curves in different colours represent the δ bounds for different combinations of ε and γ. When ε is constant, δ will increase with decreasing γ; when γ is constant, δ will increase with ε. Small δ occurs when γ is much greater than ε. High δ occurs when ε is much greater than γ. It should be remembered that, although ε and γ are theoretically independent variables, there is often fairly good correlation between them from laboratory observation (Sayers 2004). The constraints are less sensitive to the ratio of β_0/α_0 than the other Thomsen parameters. For display convenience, we assume a constant β_0/α_0 ratio of 0.55 and then plot the measured data with bounds of δ. As shown in Fig. 13, the trends of the approximated bounds comply well with the laboratory measured data if data points lying outside of the δ bounds are not displayed.

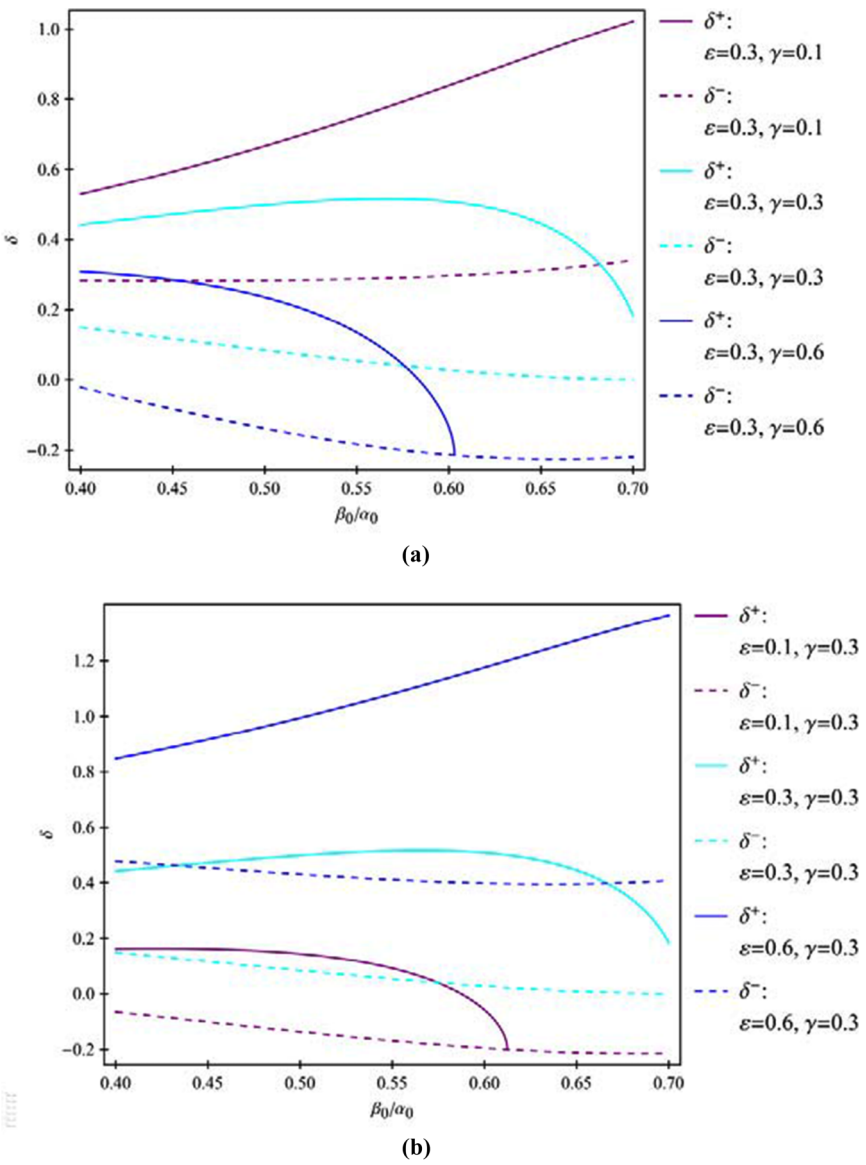

Figure 11 Relation between bounds of δ and ε, γ, and ratio of β_0/α_0. Two of the upper bounds are terminating when crossing with the low bounds due to $c_{11} - 2c_{66} < 0$, which might be non-physical.

The geometry of the bounding surfaces also clearly shows the influence of ε and γ on δ. When $c_{11} - 2c_{66} < 0$, the upper bound surface crosses the lower bound surface and disappears. Figure 12(b) shows the histogram of $c_{11} - 2c_{66}$ from laboratory velocity anisotropy measurement. Of total of 203 data points, there are only 2 data points with $c_{11} - 2c_{66} < 0$, which are from Thomsen (1986). We trace the data points to the original report (Lin 1985), and it turns out that one data point is due to data entry error and the other data point is due to signals of substandard quality. Since $c_{11} - 2c_{66} < 0$ is simultaneously derived with the upper constraints of c_{13} (equation (11)), the laboratory data validate that our assumption of $v_{HH} > 0$ is rational.

Since δ is constrained by the non-oblique properties, it might be possible that we can approximately predict δ without oblique velocity measurement. In the upper panel of Fig. 14, using data points within the bounds, we directly correlate δ with the other Thomsen parameters. Comparing the coefficients before ε, γ, and β_0/α_0 ratio, it is found that δ is more sensitive to ε and γ than the ratio of β_0/α_0; δ is positively correlated to ε and negatively correlated to γ . In the lower panel, we use the bounds of δ (equation (16)) to

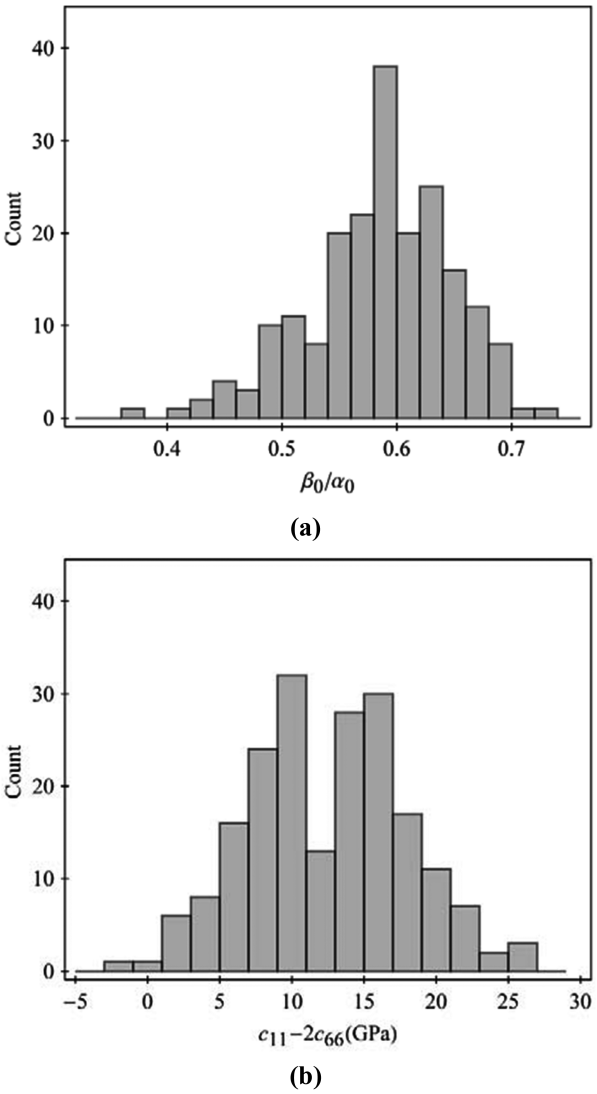

Figure 12 Distributions of (a) β_0/α_0 ratio and (b) $c_{11} - 2c_{66}$ from laboratory anisotropy measurement. Data sources same as Fig. 6.

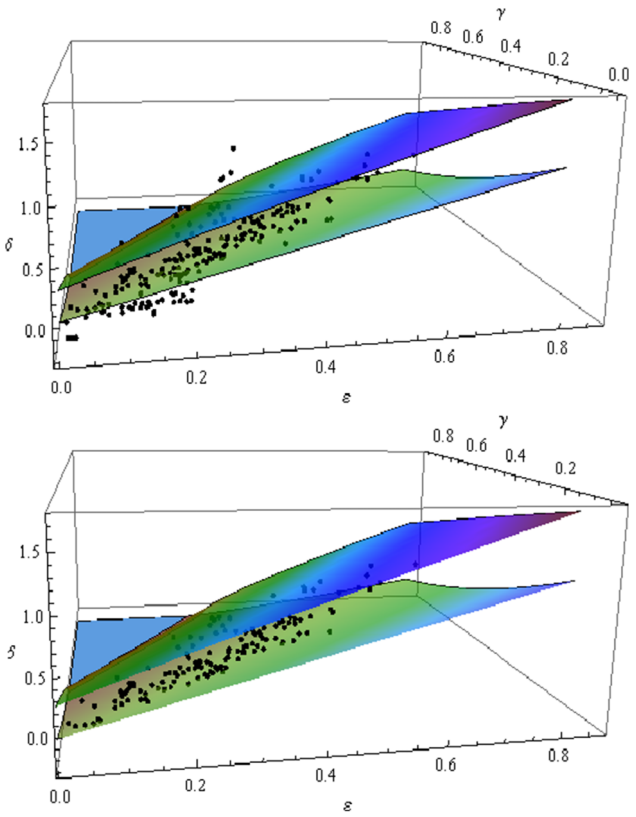

Figure 13 Comparison between estimated δ and the δ bounds using constant β_0/α_0 of 0.55. (Above, all the data points in Fig. 6 and, below, grey data points in Fig. 6 are removed).

predict δ . Considering there are a lot of data points lying out of the bounds, it is reasonable to believe that the data points within the bounds should also have significant uncertainty; thus, the prediction results are encouraging. Also it should be noted that the samples come from all over the world and are in different saturation and pressure conditions.

In practical application of anisotropic seismic data processing, the bounds on δ or η might be very useful in constraining estimation of TI parameters from seismic data. For a certain area under study, if correlation between ε and γ is established, by assuming a certain β_0/α_0 ratio, then δ can be estimated as the average of the upper bound and low bound.

DISCUSSION

The physical bounds are brought up with organic shales in mind. They should be applicable to TI sedimentary rocks caused by preferred orientation of minerals and cracks and layering effect. The intrinsic factor causing this type of TI anisotropy is the universal law of gravity. Although this type of rocks represent only a specified type of TI media, they are most common and important for oil and gas exploration. If systematic tectonic fractures cutting through the sedimentary rocks layers or beddings significantly affect the elastic properties, then they should not be approximated as TI media and the bounds we brought up in this study should not apply. The physical constraints are not applicable to TI medium with higher Young's modulus along the TI symmetry axis than that in the direction perpendicular to the symmetry axis. This type of TI medium, although rare, does exist in nature. Basalt rock with column joints (formed by thermal contraction) may be a good example of this type of TI medium. We do not suggest applying the physical constraints on individual mineral

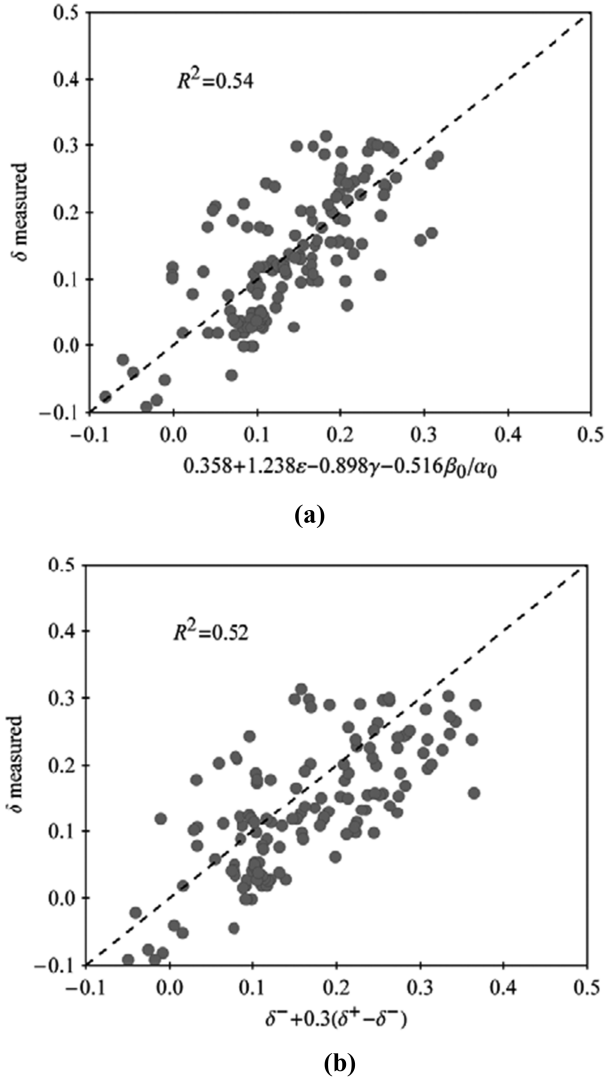

Figure 14 Prediction of δ: (a) from other Thomsen parameters and (b) from δ constraints.

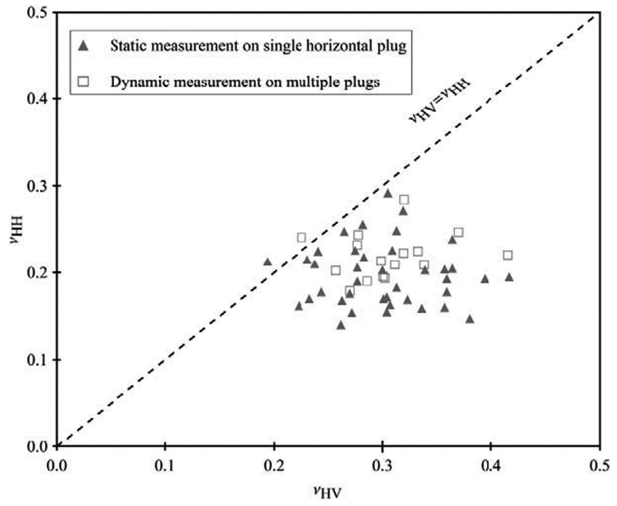

Figure 15 Relation between v_{HH} and v_{HV} from static and dynamic measurements on organic shales (data from Sone (2012, 2013)).

crystal, as special crystal lattice structure may lead to negative Poisson's ratio in a certain direction.

Since this study is focused on hydrocarbon source rocks with TI anisotropy, the assumptions about smaller Young's modulus along the TI symmetry axis than that in the direction perpendicular to the TI symmetrical axis and $c_{33} > c_{44}$ can be treated as well-known knowledge. The basic assumption for derivation of the physical bounds is $0 < v_{HH} < v_{HV}$, which is validated by reasoning and static laboratory measurements.

Rocks are usually not ideally elastic. The magnitudes of bulk modulus, shear modulus, and Young's modulus can vary depending on the magnitude and frequency of the stress applied. Poisson's ratio might also vary under dynamic and static measurements. Nevertheless, the fundamental relations between these parameters, once established, should be same for both static and dynamic measurements. For example, static measurement shows $c_{11} > c_{66}$. For dynamic measurement, c_{11} and c_{66} may both be different, but the relation $c_{11} > c_{66}$ should still hold. Figure 15 shows the crossplots between v_{HH} and v_{HV} for both static measurement and ultrasonic dynamic measurement using Sone's data (2012, 2013). The organic shale samples come from Barnett, Haynesville, and Eagle Ford shales. The data points from static measurement and dynamic measurement are different. The static measurement is based on strain measurements on a single horizontal plug, whereas the dynamic measurement is based on velocity measurements on five cylindrical plugs with angles 0°, 30°, 45°, 60°, and 90° angles to the TI symmetry axis, respectively. From Fig. 15, no matter static measurement or dynamic measurement, the overall pattern of $v_{HH} < v_{HV}$ is same.

The energy constraints on TI elastic constants are summarized by Dellinger (1991) as:

$$c_{11} > c_{66} > 0, \quad c_{33} > 0, \quad c_{44} > 0, \tag{24}$$

$$c_{13}^2 < c_{33}(c_{11} - c_{66}). \tag{25}$$

It should be noted these constraints are for a general TI medium, which does not specify $c_{11} > c_{33}$, $c_{66} > c_{44}$, and it does not require Young's modulus is lower along the TI symmetry axis than that in the direction perpendicular to the TI symmetry axis. The physical constraints on c_{13} we brought up are for a specified type of TI medium, which is stiffer along the bedding/layering than the TI symmetry axis and does not have a special network structure leading to negative Poisson's ratio;

thus, they are much tighter than the constraints by equations (24) and (25).

CONCLUSIONS

For hydrocarbon source rocks with TI anisotropy, the elastic constant c_{13} are constrained by c_{11}, c_{33}, and c_{66}. Therefore, the Thomsen parameter δ and anellipticity parameter η are constrained by the other anisotropy parameters that can be measured either along or perpendicular to the TI symmetry axis. Using these constraints, we find out that there exist significant uncertainties in laboratory velocity anisotropy measurement. Various factors causing these uncertainties are analyzed. The physical constraints on the Thomsen parameter δ can help us understand the relation between δ and the other Thomsen parameters. Generally, δ increases with ε and decreases with increasing γ. Variation of β_0/α_0 of the hydrocarbon source rocks in a certain area is usually small so that δ is less sensitive to β_0/α_0. We also show that δ can be approximately predicted by the other Thomsen parameters. The physical constraints on δ and η should also have potential application on anisotropic seismic data processing.

ACKNOWLEDGEMENTS

The authors would like to thank the Fluid/DHI consortium sponsors for supporting the consortium and this study. They also thank Hiroki Sone for sharing his dissertation data and answering their queries regarding the data. They thank the reviewers for careful reviewing of the manuscript. Especially, they would like to thank Frans Kets for very careful proofreading, many in-depth comments and good suggestions, and thank Mark Chapman for very pithy comments for improving the manuscript.

REFERENCES

Alkhalifah T. and Tsvankin I. 1995. Velocity analysis for transversely isotropic media. *Geophysics* **60**, 1550–1566.

Banik N.C. 1987. An effective anisotropy parameter in transversely isotropic media. *Geophysics* **52**, 1654–1664.

Banik N.C. 2012. Effects of VTI anisotropy on shale reservoir characterization. *SPE Middle East Unconventional Gas Conference and Exhibition*, Abu Dhabi, UAE, SPE paper 150269.

Blakslee O.L., Proctor D.G., Seldin E.J., Spence G.B. and Weng T. 1970. Elastic constants of compression annealed pyrolytic graphite. *Journal of Applied Physics* **41**, 3373–3382.

Carcione J.M. and Cavallini F. 2002. Poisson's ratio at high pore pressure. *Geophysical Prospecting* **50**, 97–106.

Chenevert M.E. and Gatlin C. 1965. Mechanical anisotropies of laminated sedimentary rocks. SPE paper 890.

Colak K. 1998. *A study on the strength and deformation anisotropy of coal measure rocks at Zonguldak Basin*. PhD thesis, Zonguldak Karaelmas University, Turkey.

Dellinger J.A. 1991. *Anisotropic seismic wave propagation*. PhD thesis, Stanford University, USA.

Dellinger J.A. and Vernik L. 1994. Do traveltimes in pulse-transmission experiments yield anisotropic group or phase velocities? *Geophysics* **59**, 1774–1779.

Dmitriev S.V., Shigenari T.S. and Abe K. 2001. Poisson ratio beyond the limits of the elastic theory. *Journal of the Physical Society of Japan* **70**, 1431–1432.

Evans K.E., Nkansah M.A., Hutchinson I.J. and Rogers S.C. 1991. Molecular network design. *Nature* **353**, 124.

Gercek H. 2007. Poisson's ratio values for rocks. *International Journal of Rock Mechanics & Mining Sciences* **44**, 1–13.

Greaves G.N., Greer A.L., Lakes R.S. and Rouxel T. 2011. Poisson's ratio and modern materials. *Nature Materials* **10**, 823–837.

Gross T.S., Nguyen K., Buck M., Timoshchuk N., Tsukrov I.I., Reznik B. *et al*. 2011. Tension-compression anisotropy of in-plane elastic modulus for pyrolytic carbon. *Carbon* **49**, 2141–2161.

Jakobsen M. and Johansen T.A. 2000. Anisotropic approximations for mudrocks: a seismic laboratory study. *Geophysics* **65**, 1711–1725.

Johnston J.E. and Christensen N.I. 1995. Seismic anisotropy of shales. *Journal of Geophysical Research* **100**, 5591–6003.

King M.S. 1964. *Wave velocities and dynamic elastic moduli of sedimentary rocks*. PhD thesis, University of California, Berkeley, USA.

Lakes R. 1991. Deformation mechanisms in negative Poisson's ratio materials: structural aspects. *Journal of Materials Sciences* **26**, 2287–2292.

Landau L.D. and Lifshitz E.M. 1970. *Theory of Elasticity*, 2nd edn. Pergamon Press, p. 14.

Lin W. 1985. Ultrasonic velocities and dynamic elastic moduli of Mesaverde rock. Lawrence Livermore National Laboratory. Rep. 20273, rev. 1.

Mavko G., Mukerji T. and Dvorkin J. 1998. *The Rock Physics Handbook*. Cambridge University Press.

Sayers C.M. 2004. Seismic anisotropy of shales: what determines the sign of Thomsen's delta parameter? *SEG Expanded Abstracts*.

Slawinski M.A., Slawinski R.A., Brown R.J. and Parkin J.M. 2000. A generalized form of Snell's law in anisotropic media. *Geophysics* **65**, 632–637.

Sondergeld C.H. and Rai C.S. 2011. Elastic anisotropy of shales. *The Leading Edge* **2011**, 325–331.

Sondergeld C.H., Rai C.S., Margesson R.W. and Whidden K.J. 2000. Ultrasonic measurement of anisotropy on the Kimmeridge Shale. *SEG Expanded Abstracts*.

Sone H. 2012. *Mechanical properties of shale gas reservoir rocks and its relation to in-situ stress variation observed in shale gas reservoirs*. PhD thesis, Stanford University, USA.

Sone H. 2013. Mechanical properties of shale-gas reservoir rocks Part–1: static and dynamic elastic properties and anisotropy. *Geophysics* **78**, D381–D392.

Thomsen L. 1986. Weak elastic anisotropy. *Geophysics* **51**, 1954–1966.

Thomsen L. 1990. Poisson was not a geophysicist. *The Leading Edge*.

Tsvankin I., 2012. *Seismic Signatures and Analysis of Reflection Data in Anisotropic Media*, 3rd edn. SEG.

Vernik L. and Liu X. 1997. Velocity anisotropy in shales: a petrophysical study. *Geophysics* **62**, 521–532.

Vernik L. and Nur A. 1992. Ultrasonic velocity and anisotropy of hydrocarbon source rocks. *Geophysics* **57**, 727–735.

Wang Z. 2002a. Seismic anisotropy in sedimentary rocks, part 1: a single-plug laboratory method. *Geophysics* **67**, 1415–1422.

Wang Z. 2002b. Seismic anisotropy in sedimentary rocks, part 2: laboratory data. *Geophysics* **67**, 1423–1430.

Yan F., Han D.-h. and Yao Q. 2012. Oil shale anisotropy measurement and sensitivity analysis. *SEG Expanded Abstracts*.

Yan F., Han D.-h. and Yao Q. 2014. Benchtop rotational group velocity measurement on shales. *SEG Expanded Abstracts*.